Chimica Techno Acta
published by Ural Federal University
eISSN 2411-1414
chimicatechnoacta.ru

ARTICLE
2024, vol. 11(4), No. 202411405
DOI: 10.15826/chimtech.2024.11.4.05

Synthesis of copper-doped nanocrystalline tin stannate by thermal decomposition of a precursor

Alexander I. Aparnev *, Anton V. Loginov, Alexander G. Bannov

Faculty of Mechanical Engineering and Technologies, Novosibirsk State Technical University, Novosibirsk 630073, Russia
* Corresponding author: aparnev@corp.nstu.ru

This paper belongs to a Regular Issue.

Abstract

Zinc hydroxostannate $ZnSn(OH)_6$, containing 5 mol.% Cu, was obtained from hydrochloric acid solutions of tin(IV), zinc and copper by adding sodium hydroxide to pH = 8–9. The thermolysis process of the obtained sample and the phase composition of the decomposition products were studied using thermal analysis, X-ray diffraction, and scanning electron microscopy. It was shown that the main stages of dehydration are completed at a temperature of about 350 °C and, as a result of thermolysis, an X-ray amorphous product is formed, from which a solid solution of copper in zinc stannate is obtained at an annealing temperature above 650 °C. At an annealing temperature of 800 °C, a mixture of nanocrystalline tin dioxide SnO_2 with a cassiterite structure and copper-doped zinc orthostannate Zn_2SnO_4 with a spinel structure is formed. The room temperature sensors based on $ZnSnO_3$ and carbon nanofibers as a conductive additive showed high response to NO_2 (–6.1% to 2 ppm NO_2).

Keywords

zinc stannate
nanocomposites
hydrous stannates
thermolysis of precursors
gas sensor

Received: 06.09.24
Revised: 25.09.24
Accepted: 25.09.24
Available online: 08.10.24

Key findings

- When precipitating tin (IV), zinc and copper hydroxides from hydrochloric acid solutions, zinc-copper hydroxostannate with the structure $ZnSn(OH)_6$ is obtained in the form of well-faceted cubic crystals.
- Optimization of the composition of the metal oxide semiconductor leads to an improvement in gas-sensitive characteristics.
- The resulting functional materials based on the products of thermolysis of the precursor $Zn_{0.95}Cu_{0.05}Sn(OH)_6$ are promising for use as heterogeneous additives in the creation of gas-sensitive sensor elements for NO_2 detection.

1. Introduction

Multicomponent metal oxide materials based on the Zn-Sn-O system have numerous functional properties, and, therefore, researchers are interested in them. For example, zinc stannate has recently been used as an anode material for sodium-ion and lithium-ion batteries [1–6]. In addition, a number of papers [7–9] noted the possibility of using stannates as materials for supercapacitors and electrodes in solar cells. Due to its chemical reactivity, excellent electronic properties and perovskite structure, $ZnSnO_3$ is widely used as a gas sensors for various substances of inorganic and organic nature [9–19]. Zinc stannates also find numerous applications in electronics, catalysis, and photocatalysis [20–27]. It is noteworthy that stannates obtained by thermal decomposition have a relatively high specific surface area (10-100 m^2/g) and can be used as functional additives for the production of composite solid electrolytes [28].

In the Zn-Sn-O system, the existence of two compounds is known: zinc metastannate $ZnSnO_3$ and zinc orthostannate Zn_2SnO_4. Zinc metastannate has an orthorhombic crystal lattice and has a crystalline structure resembling perovskite, while zinc orthostannate is characterized by a cubic lattice with a spinel structure. In order to obtain these compounds, various methods are used: low-temperature ion exchange, sol-gel technology, and co-precipitation followed by heat treatment. These include the sol-gel method, which is the most common due to its ease of control, low temperature, and high efficiency in obtaining various homogeneous nanostructures.

For practical applications, the co-deposition method is usually used, as it is more accessible and easier to implement. It was previously demonstrated that $MSn(OH)_6$ hydroxostannates and $MSnO_3$ and M_2SnO_4 oxostannates (where M = Mg, Ca, Sr, and Ba) can be obtained by thermal decomposition [9, 27–30]. In a number of works [5, 9, 13, 20, 21], it is shown that composites based on them, such as $ZnSnO_3/ZnO$, $ZnSnO_3/SnO_2$, $ZnSnO_3/Fe_2O_3$, and $ZnSnO_3/CuO$, are used to enhance the gas-sensitive characteristics of stannates due to heterojunctions formed in such systems. Particularly, the addition of such cations induced the change in the concentration of charge carrier concentration.

The present work is devoted to the study of decomposition products of the precursor zinc-copper hexahydroxostannate (with a molar copper content of 5%) and the possibility of their use as heterogeneous oxide additives to create gas sensors for NO_2 detection at room temperature.

2. Materials and Methods

In the work, the following starting reagents were used: $ZnCl_2$ (zinc chloride, purity not less than 98%), $Na_2SnO_3{\cdot}3H_2O$ (sodium stannate trihydrate, purity not less than 97%), $CuCl_2{\cdot}2H_2O$ (copper chloride dihydrate, purity not less than 98%), HCl (hydrochloric acid of high purity), and NaOH (sodium hydroxide, purity of at least 99%). Solutions of HCl and NaOH were prepared in double distilled water obtained using a laboratory BE-2 purification system. All chemicals were used in the form in which they were obtained, without additional purification.

Zinc hydroxostannate $ZnSn(OH)_6$ with a content of 5 mol.% copper(II) was synthesized by hydrolytic co-deposition by dissolving $ZnCl_2$ and $CuCl_2{\cdot}2H_2O$ in hydrochloric acid solution and adding $Na_2SnO_3{\cdot}3H_2O$ according to the following procedure. Initially, 5.57 g $ZnCl_2$ and 0.365 g $CuCl_2{\cdot}2H_2O$ were dissolved in 50 ml of a 2M hydrochloric acid solution. Next, 11.47 g $Na_2SnO_3{\cdot}3H_2O$ was added to the resulting solution, which corresponds to the atomic ratio Zn:Cu:Sn = 0.95:0.05:1. Then a 1M NaOH solution was gradually added, maintaining the acidity of the medium within a pH range of 8–9. The pH values were monitored using an HI 2221 laboratory pH meter. For complete quantitative co-precipitation of zinc, tin(IV) and copper(II) the mixture was continuously stirred for 24 h. The resulting light blue precipitate was filtered from the mother liquor, washed with distilled water until a negative qualitative reaction was achieved to the presence of Cl^- ions in the solution, and dried in a drying cabinet at 110 °C for 4 h.

The microstructure and phase composition of the samples were determined by X-ray diffraction (XRD). X-ray diffraction patterns were recorded at room temperature using a Bruker D8 Advance diffractometer with Cu Kα radiation in the 2θ range from 10 to 70°. The phases formed in the system were identified using the Crystallographica Search-Match, Version 2.1 program and the PDF4 database. The average crystallite size was estimated from diffraction line broadening in X-ray diffraction patterns using the Scherer formula:

$$d = \frac{k\lambda}{\beta \cos\theta}, \quad (1)$$

where d is the average crystallite size (Å), λ is the X-ray wavelength (1.54051 Å), β is the full width at half maximum of the diffraction peak (rad.), θ is the diffraction angle (°), and k = 0.9.

Thermal analysis (TA) of the dried powders was performed on a NETZSCH Jupiter 449C STA synchronous thermal analyzer coupled to QMS 403C Aëolos (TG-QMS) mass spectrometer in an argon flow at temperatures in the range of 20–800 °C at a heating rate of 10 C·min^{-1}. The microstructure of the samples was studied by field emission scanning electron microscopy (SEM) on a Hitachi SU8000 electron microscope. The images were taken in the secondary electron recording mode at an accelerating voltage of 2–30 kV and a working distance of 8–10 mm. The samples were analyzed by energy dispersive X-ray spectroscopy using an Oxford Instruments X-max energy dispersive spectrometer. The specific surface area was calculated from the analysis of low-temperature nitrogen adsorption isotherms at 77 K using the Brunauer-Emmett-Teller (BET) method on a Quantachrome Nova 1000e static instrument. The analysis of the chemical composition of mother liquor to determine the concentration of zinc, tin and copper was carried out using the method of inductively coupled plasma atomic emission spectrometry on a specialized setup (Agilent 7500A Inductively Coupled Plasma Mass Spectrometer).

The sensors for NO_2 detection at room temperature based on $ZnSnO_3$ were prepared using the drop casting technique. The additive (carbon nanofibers (CNFs)) was used to increase the conductivity of active layer of sensor (conductivity of stannate layer was relatively low). The suspension of $ZnSnO_3$/CNFs in ethanol was deposited on the textolite substrate (10×10 mm) with copper electrodes (8×8 mm was the area of active layer). The dispersion of powder was achieved by sonication (22 kHz, UZV-3/200 RELTEC ultrasonic bath, Yekaterinburg, Russia). The droplets were deposited on the substrate heated to 80 °C and formed the active layer, covering the copper electrodes.

The measurements of the sensor response to nitrogen dioxide was carried out using dynamic flow setup. Synthetic air (79 vol.% N_2, 21 vol.% O_2) and analyte (NO_2 diluted in synthetic air) were fed into the setup, and the change in the resistance was registered at 25±1 °C and the relative humidity 2.5±1%. The resistance of active layer was measured with a two-point technique (Keithley 2401 Source Meter). The sensor response was calculated using the following equation:

$$\Delta R/R_0 = ((R - R_0)/R_0)\cdot 100\%, \quad (2)$$

where R and R_0 are the sensor resistances in the mixture of analyte + synthetic air and pure synthetic air, respectively (Ω).

 DOI: 10.15826/chimtech.2024.11.4.05

3. Results and Discussion

According to the XRD data, only those reflections related to the phase of zinc hexahydroxostannate $ZnSn(OH)_6$ are recorded on the diffractogram (2θ = 19.75; 22.85; 32.57; 36.54; 38.40; 40.16; 46.71; 52.61; 52.65; 58.10; 62.00; 68.21) with the structure of bismirnovite (spatial symmetry group Pn3m), similar to the structure of schoenflysite with a cubic unit cell. The diffractogram of the sample is shown in Figure 1, curve 1. The value of the lattice parameter, determined using the Rietveld method with Powder Cell 2.4 software, was *a* = 0.77643±0.00082 nm, in a good agreement with literature data [9, 31–33] (*a* = 0.78 nm, PDF4, card no. 73-2384). At the same time, no individual phases containing copper were detected. It is possible that copper is contained in the form of solid solutions since there is a slight broadening and shift of the peaks in the diffraction pattern. Thus, the formation of a precursor can be represented by the following scheme:

$$0.95\ ZnCl_2 + 0.05\ CuCl_2{\cdot}2H_2O + Na_2SnO_3{\cdot}3H_2O \rightarrow Zn_{0.95}Cu_{0.05}Sn(OH)_6 + 2\ NaCl + 2\ H_2O. \quad (3)$$

The data of the inductively coupled plasma atomic emission spectrometry method on the residual content of zinc (less than 0.1 μg/mL), tin (less than 0.2 μg/mL) and copper (less than 0.1 μg/mL) in the mother liquor indicate their complete precipitation in the stoichiometric ratio Zn:Cu:Sn = 0.95:0.05:1 according to the proposed scheme.

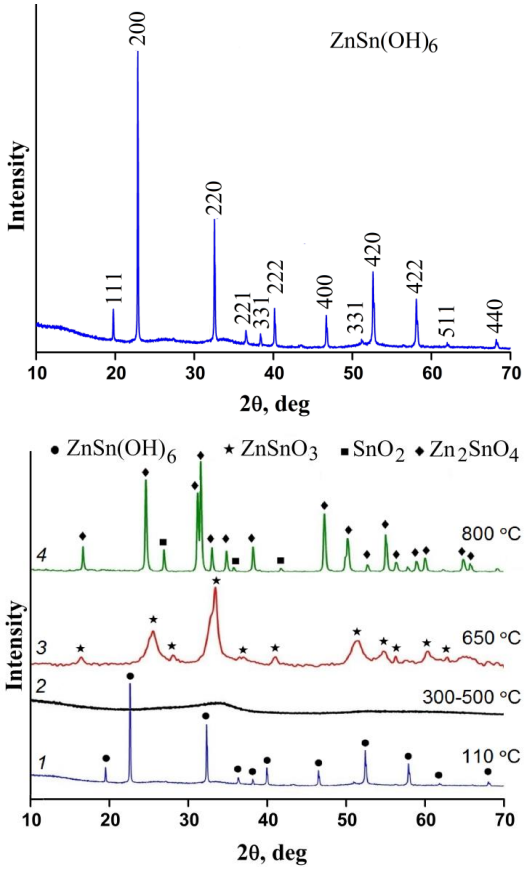

Figure 1 Diffractograms of the freshly deposited sample (*1*) and thermolysis products obtained at temperatures 300...500 (*2*), 650 (*3*) and 800 (*4*) (Cu K*α* radiation).

According to electron microscopy data (Figure 2a), freshly deposited samples $Zn_{0.95}Cu_{0.05}Sn(OH)_6$ (S = 31 m²/g) are cubic particles with a size of no more than 250 nm. The results of chemical microanalysis conducted by energy dispersion spectroscopy show that the atomic ratio Zn:Cu:Sn:O lies within (9.5±0.9):(0.5±0.05):(10±1):(64±3), that is, close to the stoichiometric ratio for $Zn_{0.95}Cu_{0.05}Sn(OH)_6$.

According to the TA data presented in Figure 3, when $Zn_{0.95}Cu_{0.05}Sn(OH)_6$ is heated, sequential processes are observed, accompanied by changes in mass, structure and phase composition, which is consistent with the results of XRD. When the sample is heated in the temperature range of 50–520° C, a mass loss of ~18.7% is observed, which is quantitatively consistent with the calculated value (18.87%) for the reaction:

$$Zn_{0.95}Cu_{0.05}Sn(OH)_6 \rightarrow Zn_{0.95}Cu_{0.05}SnO_3 + 3H_2O. \quad (4)$$

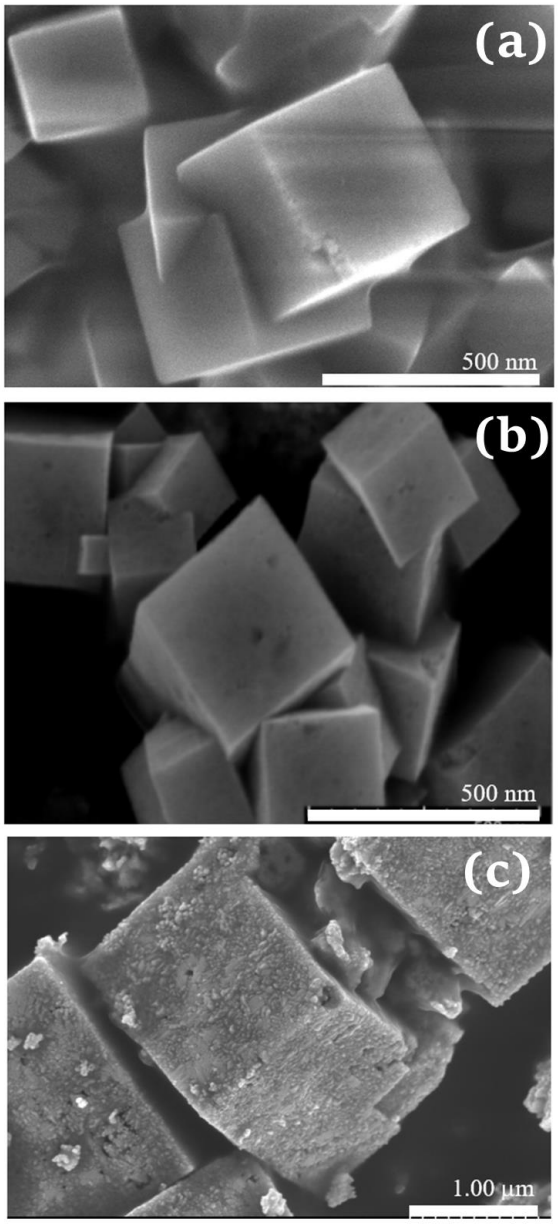

Figure 2 SEM images of the as-deposited sample (a) and after calcination at 650 °C (b) and 800 °C (c).

 DOI: 10.15826/chimtech.2024.11.4.05

The reaction is accompanied by an endothermic effect with a maximum at T_{max} = 242 °C.

Scanning electron microscopy data showed that the dehydration product is a pseudomorphosis that retains the shape of the initial particles and consists, apparently, of nanoparticles of an amorphous phase (Figure 2b). Upon further calcination at temperatures of 670–720 °C, an exothermic effect is observed, which may be associated with the formation of a weakly crystallized phase of a solid solution $Zn_{0.95}Cu_{0.05}SnO_3$ (S = 77 m²/g) with a perovskite structure and a particle size of 20–25 nm (PDF4 file No. 28-1486) (Figure 1, curve 3). At temperatures above 720 °C, apparently, as for the metastable zinc metastannate $ZnSnO_3$, there is a transition to a more stable phase of a solid solution of the composition $Zn_{1.9}Cu_{0.1}SnO_4$ with a spinel structure according to the scheme:

$$2\ Zn_{0.95}Cu_{0.05}SnO_3 \rightarrow Zn_{1,9}Cu_{0.1}SnO_4 + SnO_2. \quad (5)$$

As a result, a mixture of the nanocrystalline phase SnO_2 with a cassiterite structure with lattice parameters corresponding to pure SnO_2 (PDF4 file No.71-652) and particles of the Zn_2SnO_4 phase alloyed with copper with a spinel structure with a modified crystal lattice parameter (PDF4 file No. 74-2184) is formed (Figure 1, curve 4). The evaluation using the Scherrer equation shows that the nanocomposite consists of particles of zinc orthostannate with a size of less than 80 nm and tin dioxide with a size of 20–30 nm. According to the SEM data, the pseudomorphosis, which represents aggregates of nanoparticles, is preserved (Figure 2c). In this case, large cubic aggregates consist of weakly aggregated $Zn_{1.9}Cu_{0.1}SnO_4$ nanoparticles surrounded by smaller tin dioxide particles.

Nanocomposite powders based on $Zn_{0.95}Cu_{0.05}SnO_3$ solid solution were tested as oxide heterogeneous additives to create gas-sensitive elements of nitrogen dioxide sensors, since the sample is a good semiconductor, and a change in the concentration of charge carriers in it caused by NO_2 can provide improved sensor characteristics.

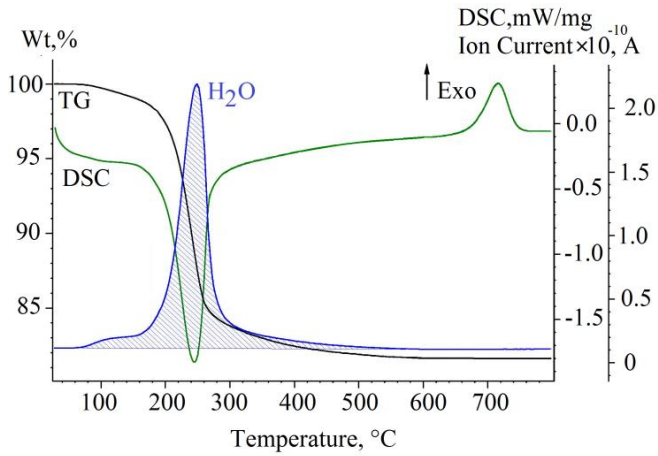

Figure 3 Synchronous thermal analysis curves obtained during thermal decomposition of the initial sample: mass change (TG), thermal effects (DSC), and ion current of the m/z = 18 amu, corresponding to water molecules released from the sample.

Figure 4 shows the reaction of sensors based on pure CNFs, a mixture of pure $ZnSnO_3$ and CNFs, a solid solution of $Zn_{0.95}Cu_{0.05}SnO_3$ and CNFs to NO_2 at room temperature.

The sensor based only on solid solution of copper in $ZnSnO_3$ possessed very small conductivity. The resistance of active layer of sensor was above hundreds of MΩ that exceeds the limit of measurement of the device (Keithley 2401 Source Meter; the setup was described in [34] in detail). Therefore, in order to decrease the resistance of stannate layer, the carbon nanofibers (CNFs) (cup stacked structure; synthesized using CVD process according to [35]) were added to $ZnSnO_3$ with the formation of hydride coating, which was sensitive to NO_2 at room temperature. The response $\Delta R/R_0$ of carbon nanofibers was around −3.9%, whereas the addition of $ZnSnO_3$ led to the increase of the sensor response. The system based on 34%$Zn_{0.95}Cu_{0.05}SnO_3$/66%CNFs showed the same response at 2 ppm NO_2, but the growth of $\Delta R/R_0$ was observed at higher concentration of nitrogen dioxide. Further increase in the fraction of stannate in the composite (50%$Zn_{0.95}Cu_{0.05}SnO_3$/50%CNFs) made it possible to increase the response at 2 ppm to −6.1%. Therefore, the addition of CNFs with conductivity higher compared to stannate makes it possible to obtain the gas sensor with higher sensor response. It can be noted that some stannates were used in gas sensors, but the issues related to the resistance of their active layer were not considered [36, 37]. Moreover, the sensitivity of the sensor based on 50%$Zn_{0.95}Cu_{0.05}SnO_3$/50%CNFs increases compared to conductive additive, i.e., CNFs. It is clearly seen from the shape of sensor curve that the response of the sensor depends on the NO_2 concentration stronger.

Considering the mechanism of nitrogen dioxide detection, it can be noted that the sensor resistance drops under NO_2 exposure. This gas is considered as electron-acceptor gas, which increases the concentration of charge carriers (holes) in the sensing material facilitating the decrease in resistance (absorption of electrons from the surface of 50%$Zn_{0.95}Cu_{0.05}SnO_3$/50%CNFs sensing material).

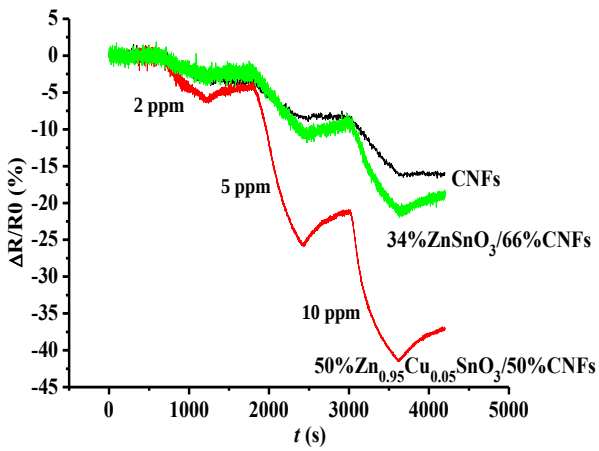

Figure 4 Sensor response of zinc stannate-based sensor to NO_2 (25±1 °C).

 DOI: 10.15826/chimtech.2024.11.4.05

4. Limitations

This work shows the possibility of using copper-doped tin stannate as an oxide heterogeneous additive in gas-sensitive sensor elements. The main problems were related to the conductivity of the sensing material, the resistance of which was high enough to detect with RLC-meter (exceeding the limit of detection). The addition of carbon additive (i.e. carbon nanofibers) with higher conductivity compared to stannate made it possible to obtain the good signal from films and measure their sensing behavior to NO2 at room temperature. Future research will focus on deeply analysing the mechanism and effect of copper addition on the performance of zinc stannate-based sensing material.

5. Conclusions

This work demonstrates that the zinc hydroxystannate powder $ZnSn(OH)_6$, containing 5 mol.% Cu and having cubic crystals no larger than 250 nm, can be obtained by precipitation from aqueous solutions containing $ZnCl_2$, $CuCl_2$, and Na_2SnO_3. During thermolysis of the initial sample, an X-ray amorphous zinc-copper stannate is formed in the temperature range of 300 to 500 °C, and at an annealing temperature of 650 °C a solid copper solution is formed in zinc stannate with a $ZnSnO_3$ structure with particle sizes of 20–25 nm and a high specific surface area of 77 m^2/g. At an annealing temperature of 800 °C, a mixture of nanocrystalline tin dioxide SnO_2 (20–30 nm) with a cassiterite structure and copper-doped zinc orthostannate Zn_2SnO_4 (less than 80 nm) with a spinel structure is formed. It was found that neither in the original sample nor in the products of its thermolysis were individual phases containing copper detected. It is likely that copper is in the form of solid solutions, as there is slight broadening and shift of the peaks observed in the diffractograms. As a result of the thermolysis study, optimal conditions for the formation of highly dispersed zinc stannate were found, and the obtained materials were subsequently used as gas sensors for room temperature detection of NO_2.

• Supplementary materials

No supplementary materials are available.

• Funding

The work was carried out in accordance with the state task of the Ministry of Education and Science of Russia (project FSUN-2023-0008).

• Author contributions

Conceptualization: A.A., A.G.
Data curation: A.L.
Formal Analysis: A.A., A.L., A.G.
Funding acquisition: A.A.
Investigation: A.A., A.L., A.G.
Methodology: A.A., A.L., A.G.
Project administration: A.A.
Resources: A.A., A.G.
Software: A.L., A.G.
Supervision: A.G.
Validation: A.A., A.L., A.G.
Visualization: A.A., A.L., A.G.
Writing – original draft: A.A., A.L., A.G.
Writing – review & editing: A.A., A.L., A.G.

• Conflict of interest

The authors declare no conflict of interest.

• Additional information

Author IDs:
Alexander I. Aparnev Scopus ID 7801309186;
Anton V. Loginov, Scopus ID 57189525710;
Alexander G. Bannov, Scopus ID 54788777600.

Website:
Novosibirsk State Technical University, https://en.nstu.ru/.

References

1. Li X, Guan G, Yu C, Cheng B, Chen X, Zhang K, Xiang J. Enhanced electrochemical performances based on $ZnSnO_3$ microcubes functionalized in-doped carbon nanofibers as free-standing anode materials. Dalton Trans. 2023;52(32):11187–11195. doi:10.1039/D3DT01642K
2. Zhang Y, Wei J-L, Jin X-Y, Yu M-C, Wang L, Guo Yu-H, Dong S-T. Electrospun $ZnSnO_3$/C Nanofibers as an Anode Material for Lithium-Ion Batteries. J Electron Mater. 2021;50:4945–4953. doi:10.1007/s11664-021-09036-x.
3. Ma Y, Jiang R, Li D, Dong Y, Liu Y, Zhang J. Embedding ultrafine $ZnSnO_3$ nanoparticles into reduced graphene oxide composites as high-performance electrodes for lithium ion batteries. Nanotechnol. 2018;29(19):195401. doi:10.1088/1361-6528/aab07e
4. Wang D, Pu X, Yu X, Bao L, Cheng Y, Xu J, Han S, Ma Q, Wang X. Controlled preparation and gas sensitive properties of two-dimensional and cubic structure $ZnSnO_3$. J Colloid Interface Sci. 2022 608(1):1074–1085. doi:10.1016/j.jcis.2021.09.167
5. Wei JL, Jin XY, Yu MC, Wang L, Guo YH, Dong ST, Zhang YM. Electrospun $ZnSnO_3$/C nanofibers as an anode material for lithium-ion batteries. J Electron Mater. 2021;50:4945–4953. doi:10.1007/s11664-021-09036-x
6. Wang K, Zhang S, Hou Z, Wang L, An P, Jia J, Li Y, Zhang P. Nanofibrous $ZnSnO_3$/C composite derived from natural cellulose substance as an enhanced lithium-ion battery anode. Mater. Lett. 2023;331:133435. doi:10.1016/j.matlet.2022.133435
7. Sim CK, Majid SR, Mahmood NZ. Synthesis of highly porous carbon/$ZnSnO_3$ composite and its electrochemical properties. J Energy Storage. 2020;32:101843. doi:10.1016/j.est.2020.101843
8. Sim CK, Majid SR, Mahmood NZ. $ZnSnO_3$/ mesoporous biocarbon composite towards sustainable electrode material for energy storage device. Microchem J. 2021;164:105968. doi:10.1016/j.microc.2021.105968

9. Rahman M, Bashar MS, Rahman Md. L, Chowdhury FI. Comprehensive review of micro/nanostructured $ZnSnO_3$: characteristics, synthesis, and diverse applications. RSC Advances. 2023;13(44):30798–30837. doi:10.1039/ d3ra05481k
10. Ma X, Dong X, Li B, Zheng Q, Li R, Huang C, Huo L, Zhang X, Cheng X, Xu Y. Construction of amorphous $ZnSnO_3$ micro/nano-structure material for low concentration n-pentanol detection. Ceram Int. 2024;50:25122–25130. doi:10.1016/j.ceramint.2024.04.241
11. Sun B, Sima Z, Wang Q, Song P. Effect of in doping on the formaldehyde sensing performance of $ZnSnO_3$ cubes ceramics. Ceram Int. 2023;49:39588–39596. doi:10.1016/j.ceramint.2023.09.310
12. Jiang L, Xue K, Chen Z, Cui Q, Xu S. High performance of gas sensor based on Bi-doped $ZnSnO_3$/CuO nanocomposites for acetone. Microporous Mesoporous Mater. 2022;329:111532. doi:10.1016/j.micromeso.2021.111532
13. Yu S, Jia X, Yang J, Wang S, Li Y, Song H. Highly sensitive ethanol gas sensor based on CuO/$ZnSnO_3$ heterojunction composites. Mater Lett. 2021;291:129531. doi:10.1016/j.matlet.2021.129531
14. Sun C, Shao J, Wang Z, Liu H, Li Z, Zhang H, Bai T, Sun Y, Guo L, Pan G, Yang X. CuO-sensitized amorphous $ZnSnO_3$ hollow-rounded cubes for highly sensitive and selective H_2S gas sensors. Sens Actuators B Chem. 2022;362:131799. doi:10.1016/j.snb.2022.131799
15. Gao S, Wang C , Li X, Yuan R, Zhang Q, Zhao J, Chu H. Amorphous $CoSnO_3$ for conductometric triethylamine gas sensing. Sens Actuators B Chem. 2024;401:135086. doi:10.1016/j.snb.2023.135086
16. Yan S, Zhang S-Z, Xie W-F, Gai L-Y, Yuan H-M, Zhang D, Zhang H, Liu X, Yang W, Chi Z-T. Chemiresistive ethanol sensors based on In_2O_3/$ZnSnO_3$ nanocubes. Sens Actuators Rep. 2022;4:100099. doi:10.1016/j.snr.2022.100099
17. Wang XY, Wang MM, Xin JH, Yang Z, Leng BX. The enhanced practicability of $ZnSnO_3$ sensors based on Co, Ni co-doping and N719 dye sensitization. Sens Actuators B Chem. 2022;362:131787. doi:10.1016/j.snb.2022.131787
18. Zheng J, Hou H, Fu H, Gao L, Liu H. Size-controlled synthesis of porous $ZnSnO_3$ nanocubes for improving formaldehyde gas sensitivity. RSC Adv. 2021;11:20268–20277. doi:10.1039/d1ra01852c
19. Liu K, Zheng Z, Xu J, Zhang C. Enhanced visible light-excited $ZnSnO_3$ for room temperature ppm-level CO_2 detection. J Alloys Compd. 2022;907:164440. doi:10.1016/j.jallcom.2022.164440
20. Ochoa-Muñoz YH, Rodríguez-Páez JE, Mejía de Gutiérrez R. Structural and optical study of perovskite nanoparticles $MSnO_3$ (M = Ba, Zn, Ca) obtained by a wet chemical route. Mater Chem Phys. 2021;266:124557. doi:10.1016/j.matchemphys.2021.124557
21. Martínez-Aguilar E, Hmŏk H'L, Siqueiros JM, López-Juárez R. Tuning of the ferroelectric and optical properties of $ZnSnO_3$ with transition metals: Mn, Cr and Co. Mater Chem Phys. 2024;319:129387. doi:10.1016/j.matchemphys.2024.129387
22. Li D, Yan P, Zhao Q, Wang L, Ma X, Xue J, Zhang Y, Liu M. The hydrothermally synthesis of $ZnSn(OH)_6$ and Zn_2SnO_4 and their photocatalytic performances. Cryst Eng Comm. 2020;20:4923–4932. doi:10.1039/d0ce00777c
23. Wu Z, Fan B, Zhang L, Yao Y, Hong S, Yu H, Jia Y. Strongly enhanced piezoelectric-catalysis of $ZnSnO_3$ /graphite hybrid materials for dye wastewater decomposition. Ceram Int. 2023;49(18):29614–29621. doi:10.1016/j.ceramint.2023.06.180
24. Najorka J, Kleppe AK, Welch MD. The effect of pressure and composition on Cu-bearing hydroxide perovskite. Phys Chem Minerals. 2019;46:877–887. doi:10.1007/s00269-019-01047-9
25. Anucha CB, Altin I, Bacaksiz E, Stathopoulos VN, Polat I, Yasar A, Yüksel ÖF. Silver doped zinc stannate (Ag-$ZnSnO_3$) for the photocatalytic degradation of caffeine under UV irradiation. Water. 2021;13:1290. doi:10.3390/w13091290
26. Soltani A, Djani F, Mazouzi DE, Tiri RNE, Aygün A, Şen F, Martinez-Arias A. $ZnSnO_3$-SnO_2 nanocomposite as a ca-talyst for efficient hydrogen production through sodium borohydride methanolysis. Int J Hydrog Energy. 2024;67:429–437. doi:10.1016/j.ijhydene.2024.04.208
27. Mayedwa N, Mongwaketsi N, Khamlich S, Kaviyarasu K, Matinise N, Maaza M. Green synthesis of zin tin oxide ($ZnSnO_3$) nanoparticles using Aspalathus Linearis natural extracts: structural, morphological, optical and electrochemistry study. Appl Surf Sci. 2018;446:250–257. doi:10.1016/j.apsusc.2017.12.161
28. Loginov AV, Mateyshina YG, Aparnev AI, Uvarov NF. Synthesis of $BaSnO_3$/SnO_2 nanocomposites as heterogeneous additive for composite solid electrolytes. Russ J Appl Chem. 2018;91(10):1660–1664. doi:10.1134/S1070427218100130
29. Loginov AV, Aparnev AI, Uvarov NF. Synthesis of $SrSnO_3$/SnO_2 composites via thermal decomposition of a precursor. Inorg Mater. 2022;58(8):420–424. doi:10.1134/S0020168522040094
30. Loginov AV, Aparnev AI, Uvarov NF. Nanocomposites Prepared via Thermal Decomposition of Calcium Hydroxystannate $CaSn(OH)_6$. Inorg Mater. 2022;58(8):814–821. doi:10.1134/S0020168522080088
31. Dong S, Cui L, Zhao Y, Wu Y, Xia L, Su X, Zhang C, Wang D, Guo W, Sun J. Crystal structure and photocatalytic properties of perovskite $MSn(OH)_6$ (M = Cu and Zn) composites with d^{10}-d^{10} configuration. Appl Surf Sci. 2019;463:659–667. doi:10.1016/j.apsusc.2018.09.006
32. Marshukova NK, Palovskii AB, Sidorenko GA, Chistyakova NI. Vismirnovite, $ZnSn(OH)_6$, and natanite, $FeSn(OH)_6$, new tin minerals. Zap Vses Mineral Obshch. 1981;110:492–500.
33. Yasser H, Rodriguez-Paez JE, Gutierrez RM. Structural and optical study of perovskite nanoparticles $MSnO_3$ (M = Ba, Zn, Ca) obtained by a wet chemical route. Mater Chem Phys. 2021;266:124557. doi:10.1016/j.matchemphys.2021.124557
34. Bannov AG, Lapekin NI, Kurmashov PB, Ukhina AV, Manakhov A. Room-Temperature NO_2 Gas Sensors Based on Granulated Carbon Nanofiber Material. Chemosensors. 2022;10(12):525. doi:10.3390/chemosensors10120525
35. Kuvshinov GG, Mogilnykh YI, Kuvshinov DG. Kinetics of carbon formation from CH_4-H_2 mixtures over a nickel containing catalyst. Catal Today. 2021;42:357–360. doi:10.1016/S0920-5861(98)00115-1
36. Sivapunniyam A, Wiromrat N, Myint MTZ, Dutta J. High-performance liquefied petroleum gas sensing based on nanostructures of zinc oxide and zinc stannate. Sensors Actuators B Chem. 2011;157:232–239. doi:10.1016/j.snb.2011.03.055
37. Ganesan M, Jayaraman V, Selvaraj P, Mani KM, Kim DH. Pyrochlore cerium stannate ($Ce_2Sn_2O_7$) for highly sensitive NO_2 gas sensing at room temperature. Appl Surf Sci. 2023;624:157135. doi:10.1016/j.apsusc.2023.157135